Inorganic Chemistry

Article

pubs.acs.org/IC

Novel Garnet-Structure $Ca_2GdZr_2(AlO_4)_3:Ce^{3+}$ Phosphor and Its Structural Tuning of Optical Properties

Xinghong Gong,[†,‡] Jianhua Huang,[†] Yujin Chen,[†] Yanfu Lin,[†] Zundu Luo,[†] and Yidong Huang*[,†]

[†]Key Laboratory of Optoelectronic Materials Chemistry and Physics, Fujian Institute of Research on the Structure of Matter, Chinese Academy of Sciences, Fuzhou, Fujian 350002, China

[‡]University of the Chinese Academy of Sciences, Beijing, 100039, China

Supporting Information

ABSTRACT: Aluminate garnet phosphors $Ca_2GdZr_2(AlO_4)_3:Ce^{3+}$ (CGZA:Ce^{3+}) for solid-state white lighting sources are reported. The crystal structure and Mulliken bonding population of the CGZA:Ce^{3+} have been analyzed. The larger 5d (^{2}D) barycenter shift ε_c and smaller phenomenological parameter $10D_q$ of Ce^{3+} in CGZA are related to the larger covalent character of Ce−O. The tuning spectral properties of the Ce^{3+}-doped CGZA-based isostructural phosphors are presented. The splitting of cubic crystal field energy level ^2E_g in $Ca_2REZr_2(AlO_4)_3:Ce^{3+}$ (CREZA:Ce^{3+}) (RE = Lu, Y, and Gd) increases as the radius of RE^{3+} increases, and the splitting of ^2E_g may dominate the difference of spectroscopic red-shift $D(A)$ in CREZA:Ce^{3+}. The splitting of the ^2E_g in $CaGd_2ZrSc(AlO_4)_3:Ce^{3+}$ (CGZSA:Ce^{3+}) phosphors increases seemly due to the decreasing of the covalent character of Ce−O. Thermal quenching properties of Ce^{3+}-doped CGZA-based isostructural phosphors are also presented and analyzed. For CREZA:Ce^{3+} phosphors, the increasing of the radius of RE^{3+} results in an enhancement of thermal quenching. The quenching of CGZSA:Ce^{3+} is obviously stronger mainly due to the smaller energy difference between the lowest 5d excited state and 4f ground state.

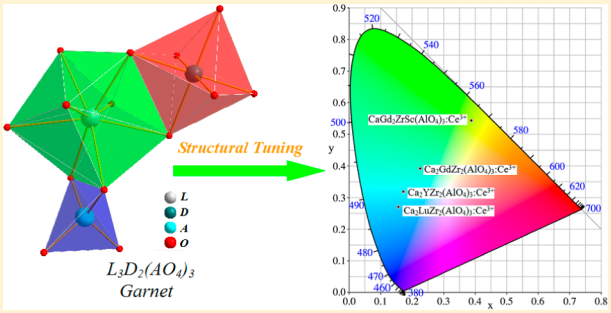

1. INTRODUCTION

Phosphor-converted white light emitting diode (pc-WLED) is regarded as one of the most promising eco-friendly light sources.[1,2] The Ce^{3+} as an activator for phosphor has the lowest 5d state among the trivalent rare earth ions, and the broad absorption and emission bands from the allowed 4f↔5d transitions can even shift from ultraviolet to visible wavelength in some host, especially in garnet crystals.[3,4]

It is well-known that garnets with formula unit of $L_3D_2(AO_4)_3$ belong to the $Ia\bar{3}d$ space group. There are three different crystallographic sites for the cations in the $L_3D_2(AO_4)_3$, L sites with eight-coordinate in dodecahedron, D sites with six-coordinate in octahedron, and A sites with four-coordinate in tetrahedron.[5] Ce^{3+}-doped garnets have been developed as green, yellow, and even red phosphors via L, D, and A chemical substitutions with different ions.[6−8] YAG:Ce^{3+} is the most frequently used yellow phosphor after it was reported in 1967 by Balsse and Bril.[7] $Ca_3Sc_2(SiO_4)_3:Ce^{3+}$ and $Lu_2CaMg_2(SiO_4)_3:Ce^{3+}$ garnets also have been developed as green and yellow-orange phosphors, respectively, in recent years.[6,8]

In this work, a series of Ce^{3+}-doped isostructural aluminate garnet phosphors containing zirconium, such as $Ca_2REZr_2(AlO_4)_3:Ce^{3+}$ (RE = Lu, Y, and Gd) and $CaGd_2ZrSc(AlO_4)_3:Ce^{3+}$, have been synthesized by the solid-state reaction method. The structure of the representative compound $Ca_2GdZr_2(AlO_4)_3$ (CGZA) has been determined to understand the detailed ions distribution in these garnet crystals. The Mulliken bonding population of the CGZA:Ce^{3+} also has been calculated by density functional theory (DFT) to evaluate the bond character of Ce−O. The photoluminescence properties of these Ce^{3+} doped CGZA-based isostructural phosphors are presented and analyzed on the basis of the crystal structure and bond character of Ce−O.

2. EXPERIMENTAL PROCEDURE

A series of powder samples of Ce^{3+}-doped aluminate phosphors listed in Table 1 were prepared using the solid-state reaction method from $CaCO_3$ (AR), $SrCO_3$ (AR), $BaCO_3$ (AR), La_2O_3 (99.99%), Gd_2O_3 (99.99%), Lu_2O_3 (99.99%), Y_2O_3 (99.99%), Sc_2O_3 (99.99%), ZrO_2 (AR), Al_2O_3 (AR), and CeO_2 (99.99%) according to the stoichiometric ratio of each sample. The powder reagents were ground together and heated at about 1500−1600 °C for 6−8 h under a reducing atmosphere of H_2/N_2 (5%/95%). The small single crystal of CGZA for structure analysis was obtained by keeping the powder reagents at 1600 °C for 5 days. The X-ray powder diffraction (XRD) data of the samples were obtained by a Rigaku MiniFlex II X-ray diffractometer over an angular range of $5° \le 2\theta \le 80°$ with a step size of 0.03°. The crystal structure of CGZA was determined by a Rigaku mercury 70 CCD diffractometer equipped with a graphite-mono-

Received: January 26, 2014
Published: June 10, 2014

   dx.doi.org/10.1021/ic500153u | Inorg. Chem. 2014, 53, 6607−6614

Table 1. List of Sample Compositions

sample	compositions	phase
CGZA:Ce^{3+}	$Ca_2Gd_{1-x}Zr_2(AlO_4)_3$:$xCe^{3+}$ (x = 0.01, 0.02, 0.04, ...0.12)	garnet
CLuZA:Ce^{3+}	$Ca_2Lu_{0.98}Zr_2(AlO_4)_3$:$0.02Ce^{3+}$	garnet
CYZA:Ce^{3+}	$Ca_2Y_{0.98}Zr_2(AlO_4)_3$:$0.02Ce^{3+}$	garnet
CLaZA:Ce^{3+}	$Ca_2La_{0.98}Zr_2(AlO_4)_3$:$0.02Ce^{3+}$	mixed
CSGZA:Ce^{3+}	$CaSrGd_{0.98}Zr_2(AlO_4)_3$:$0.02Ce^{3+}$	mixed
CBGZA:Ce^{3+}	$CaBaGd_{0.98}Zr_2(AlO_4)_3$:$0.02Ce^{3+}$	mixed
CGZSA:Ce^{3+}	$CaGd_{1.98}ZrSc(AlO_4)_3$:$0.02Ce^{3+}$	garnet

chromated Mo Kα radiation (λ = 0.71073 Å) at 293 K. The measured intensities were corrected for Lorentz and polarization factors. The absorption corrections were performed using the multiscan method. The structure was solved by the direct methods with SHELXS-97[9] and refined by full-matrix least-squares fitting on F^2 by SHELX-97.[10] Photoluminescence (PL) and photoluminescence excitation (PLE) spectra of the powder phosphors were measured using a Cary Eclipse fluorescence spectrometer at room temperature. The temperature-dependent luminescent spectra were measured using a spectrometer (FL920, Edinburgh) equipped with a homemade heating cell under the excitation of a xenon lamp. The photoluminescence quantum yields of the samples in the visible region (400−800 nm) were measured using a $BaSO_4$ coated integrating sphere in the FLS920 spectrometer.

The Mulliken bonding population analyses[11] of CGZA:Ce^{3+} as well as GdAG:Ce^{3+} for comparison were achieved by using the CASTEP code,[12,13] which relies on a plane-wave-based DFT approach. Electron correlation effects were modeled using the Perdew−Burke−Ernzerhof (PBE) generalized gradient approximation (GGA). Core electrons were replaced by norm-conserving pseudopotentials. For geometry optimizations, a plane wave with cutoff energy of 330 eV was employed. Convergence tolerance thresholds values were set to 2×10^{-6} eV/atom for the total energy, 5×10^{-2} eV/Å for the maximum ionic force, and 2×10^{-3} Å for the maximum ionic displacement. The special points sampling integration over the Brillouin zone was employed by using the Monkhorst−Pack (MP) method with 1 × 1 × 1 special k-point meshes.

3. RESULTS AND DISCUSSION

3.1. Phase Formation of Aluminate Garnet Containing Zirconium. The powder X-ray diffraction patterns of the obtained aluminate phosphors containing zirconium as well as the simulated XRD patterns of YAG from the crystal structure data[6] for comparison are shown in Figure 1. It can be found that the compounds CGZA, $Ca_2YZr_2(AlO_4)_3$ (CYZA), $Ca_2LuZr_2(AlO_4)_3$ (CLuZA), and $CaGd_2ZrSc(AlO_4)_3$ (CGZSA) are isostructural with YAG and can be indexed to the cubic system with space group $Ia\bar{3}d$ (SG 230), but many impurity phases exist in the $CaSrGdZr_2(AlO_4)_3$ (CSGZA), $CaBaGdZr_2(AlO_4)_3$ (CBGZA), and $Ca_2LaZr_2(AlO_4)_3$ (CLaZA). Generally, the stability of the garnet structure depends upon the radii of the contained cations. For example, the garnets $RE_3Al_2(AlO_4)_3$ (RE = Gd−Lu, Y) are thermodynamically stable for the rare-earth ions smaller than Gd^{3+}, but those that contain ions larger than Gd^{3+} (La^{3+}−Eu^{3+}) are not.[14−16] In this work, Ca^{2+}, which is larger than Gd^{3+}, has been introduced into the L sites of garnet structure with Zr^{4+} larger than Al^{3+} introduced to the D sites. Furthermore, the cations Zr^{4+} at D sites can also be substituted by Sc^{3+} with similar radius partly to form the CGZSA compound, and the garnet lattices are still stable. However, further expansion of the host lattice by introducing cations such as La^{3+}, Sr^{2+}, and Ba^{2+} larger than Ca^{2+} to the L sites destabilizes formation of the garnet containing zirconium.

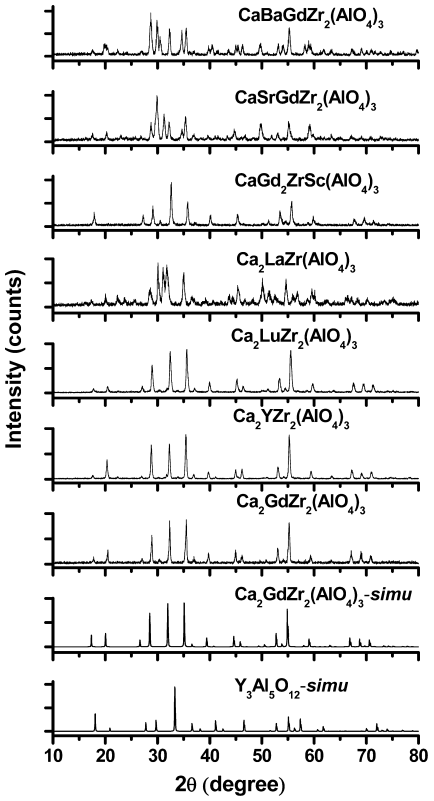

Figure 1. X-ray powder diffraction patterns of the aluminate phosphors containing zirconium and YAG.

3.2. Structure Characteristics of CGZA. To understand the detailed ion distribution in the garnet crystal, the structure of CGZA crystal was analyzed as a representative compound. The diffraction data of CGZA crystal can be indexed to the cubic system. For the final acceptable refinement, which relates to a lower R factor, the Al^{3+} ions occupy the A sites, the larger Zr^{4+} ions occupy the D sites, and the largest Ca^{2+} and Gd^{3+} ions occupy the L sites with a ratio of 2:1. The simulated XRD patterns of CGZA from the crystal structure data are also given in Figure 1 for comparison. The crystallographic data and structure refinement for the CGZA crystal are listed in Table 2. The atomic coordinates and isotropic thermal parameters are listed in Table 3.

Figure 2a displays the central projection (perspective) of a unit cell of CGZA crystal along the (001) axis. The 24c, 16a, and 24d Wyckoff sites are fully occupied by Ca^{2+}/Gd^{3+}, Zr^{4+}, and Al^{3+}, respectively. The AlO_4 tetrahedrons, which link the cations between them, are isolated from each other. Every Ca/Gd is surrounded by four $(Ca/Gd)O_8$, four ZrO_6, and six AlO_4 polyhedrons, which means that every coordination O^{2-} anion of Ca/Gd is shared by four cations, one Zr^{4+}, one Al^{3+}, and two Ca^{2+}/Gd^{3+}, as shown in Figure 2b.

The selected interatomic distances and the values of bond valence sum (BVS)[17] of CGZA are listed in Table 4. In CGZA crystal, the bond valence for Gd^{3+} ions is lower than the normal value of 3, but for Ca^{2+} it is slightly higher than the normal value of 2. It is known that bond valences are associated with bond distances. Higher or lower bond valence means that the space occupied by an ion is smaller or larger than the normal space for it. Considering the radius of Ca^{2+} is larger than that of Gd^{3+} and the bond distances obtained from X-ray diffraction are average values, the departure of bond valences from the

dx.doi.org/10.1021/ic500153u | Inorg. Chem. 2014, 53, 6607−6614

Table 2. Crystallographic Data and Structure Refinement for CGZA

empirical formula	$Ca_2GdZr_2(AlO_4)_3$
formula wt	692.79
temp (K)	293(2)
wavelength (Å	0.71073
crystal system	cubic
space group	$Ia\bar{3}d$
unit cell dimensions (Å)	a = 12.5057(7)
volume (Å^3)	1955.88(19)
Z	8
calcd density (g/cm^3)	4.706
abs coeff (mm^{-1})	10.184
F(000)	2552
crystal size (mm)	0.2 × 0.1 × 0.05
θ range for data collection (deg)	3.99−27.5
limiting indices	$-16 \le h \le 15$, $-16 \le k \le 15$, $-16 \le l \le 15$
reflns collected/unique	6371/192 [R_{int} = 0.0431]
completeness to θ = 27.47°	100%
max and min transmission	1.0000 and 0.5992
abs correction	none
refinement method	full-matrix least-squares on F^2
data/restraints/parameters	192/0/19
GOF on F^2	1.164
final R indices [$I > 2\sigma(I)$]	R_1 = 0.0162, wR_2 = 0.0417
R indices (all data)	R_1 = 0.0162, wR_2 = 0.0417
extinction coeff	0.00087(7)
largest diff. peak and hole	0.309 and −0.400 e Å^{-3}

normal values for both Ca^{2+} and Gd^{3+} also indicates that Ca^{2+} and Gd^{3+} occupy L sites simultaneously to some extent. The BVS of Al^{3+} cation at A site in CGZA is lower than the normal value of 3, which means that the Al−O bond length in the crystal is longer slightly than that in a usual compound containing $[AlO_4]^{5-}$ group, such as Sr_2EuAlO_5 (BVS = 3.003).[18] The BVS values of Zr^{4+} ion at D sites are close to the normal value of 4. The selected bond angles of CGZA and REAG (RE = Y, Gd) crystals are listed in Table 5 for comparison. It is worth noting that the α, β, and δ in LO_8 dodecahedron as shown in Figure 2c are different in order, that is, $\alpha < \beta < \delta$ in CGZA but $\beta < \alpha < \delta$ in REAG. That is, the shapes of LO_8 dodecahedron in the CGZA and REAG are different.

3.3. Chemical Bond Characteristics. The covalency between the anion ligands and Ce^{3+} ion would not only reduce energy level splitting of d electrons caused by the crystal field, spin−orbit interaction, and Jahn−Teller coupling effect, but also shift down the barycenter of 5d (^{2}D) states.[19−22] The covalent character of Ce−O bonds in garnets is affected by the cations at L, D, and A sites because the O^{2-} anion connected with Ce^{3+} is also shared by the other three cations. Increasing the electronegativety of cations at L, D, and A sites may decrease the covalent character of Ce−O bonds in Ce^{3+}-doped garnets. However, it is difficult to make a prediction about the changing trend of covalent character of Ce−O bonds in CREZA:Ce^{3+} (RE = Lu, Y, and Gd) from that in REAG:Ce^{3+} because the average electronegativity of cations at L sites is decreased due to the RE^{3+} substituted by Ca^{2+}/RE^{3+}, but the electronegativity of cations at D sites is increased due to the Al^{3+} substituted by Zr^{4+}. Therefore, the Mulliken bonding population analyses of CGZA:Ce^{3+} as well as GdAG:Ce^{3+} for comparison have been performed by DFT to evaluate the covalent character of Ce−O bond in both garnets. The supercell models used in the DFT calculation are shown in Figure 3. The nominal formulas for the supercell models are $Ca_2Gd_{0.75}Ce_{0.25}Zr_2(AlO_4)_3$ and $Gd_{2.75}Ce_{0.25}Al_2(AlO_4)_3$, respectively. The calculated values of the Mulliken bond population and bond length are listed in Table 6. It is worth noting that the covalent character of Ce−O bond in CGZA:Ce^{3+} is larger than that in GdAG:Ce^{3+}; even the Zr^{4+} with larger electronegativity has been introduced to D site, and which indicates that the Ca^{2+} with smaller electronegativity at L site dominates the covalent character of Ce−O bonds in CGZA:Ce^{3+}. Consequently, the combined effect of RE^{3+} being substituted by Ca^{2+}/RE^{3+} and Al^{3+} being substituted by Zr^{4+} to form CREZA from REAG increases the covalent character of the Ce−O bond in CREZA.

3.4. Spectral Property of CGZA:Ce^{3+}. Figure 4 shows the energy level scheme for Ce^{3+} in garnet. The barycenter of 5d (^{2}D) state as a free ion would shift down to the T_d position due to the nephelauxetic effect[19,20,22] closely related to the covalency between Ce^{3+} and O^{2-} ligands. The splitting of the 5d (^{2}D) state in garnets can be related to a $^2T_{2g}$−^2E_g cubic crystal field splitting with the additional splitting due to the distortion of the cubic coordination into a dodecahedron with D_2 symmetry.[23] In general, the absorption in Ce^{3+}-doped garnet phosphor is caused by the transitions from the $^2F_{5/2}$ multiplet of 4f configuration to the five energy levels of 5d (^{2}D) state, and the visible light emission is related to the transitions from the lowest-lying level $^2A_{1g}$ to the $^2F_{7/2}$ and $^2F_{5/2}$ multiplets.[24−26] Figure 5c shows the normalized PL and PLE spectra of the CGZA:0.02Ce^{3+} garnet phosphor. The broad luminescence band of CGZA:Ce^{3+} with peak wavelength of 500 nm exhibits the potential as a useful green phosphor for general lighting. The asymmetric emission band is fitted as a sum of two components using a Gaussian least-squares fitting, and the splitting between the $^2F_{7/2}$ and $^2F_{5/2}$ multiplets is estimated to be 1973 cm^{-1}. Two bands corresponding to excitations from $^2F_{5/2}$ multiple to the two lowest-lying levels $^2A_{1g}$ and $^2B_{1g}$ of 5d

Table 3. Atomic Coordinates and Isotropic Thermal Parameters for CGZA

atom	Wyck.	x	y	z	SOF	U_{eq}[a]
Zr	16a	0.25	0.75	0.25		0.0005(1)
Gd	24c	0.25	0.625	0	1/3	0.0007(1)
Ca	24c	0.25	0.625	0	2/3	0.0007(1)
Al	24d	0.25	0.375	0		0.0004(1)
O	96h	0.3453(2)	0.4666(2)	0.0523(2)		0.0008(1)

[a] U_{eq} is defined as one-third of the trace of the orthogonalized U_{ij} tensor.

dx.doi.org/10.1021/ic500153u | Inorg. Chem. 2014, 53, 6607−6614

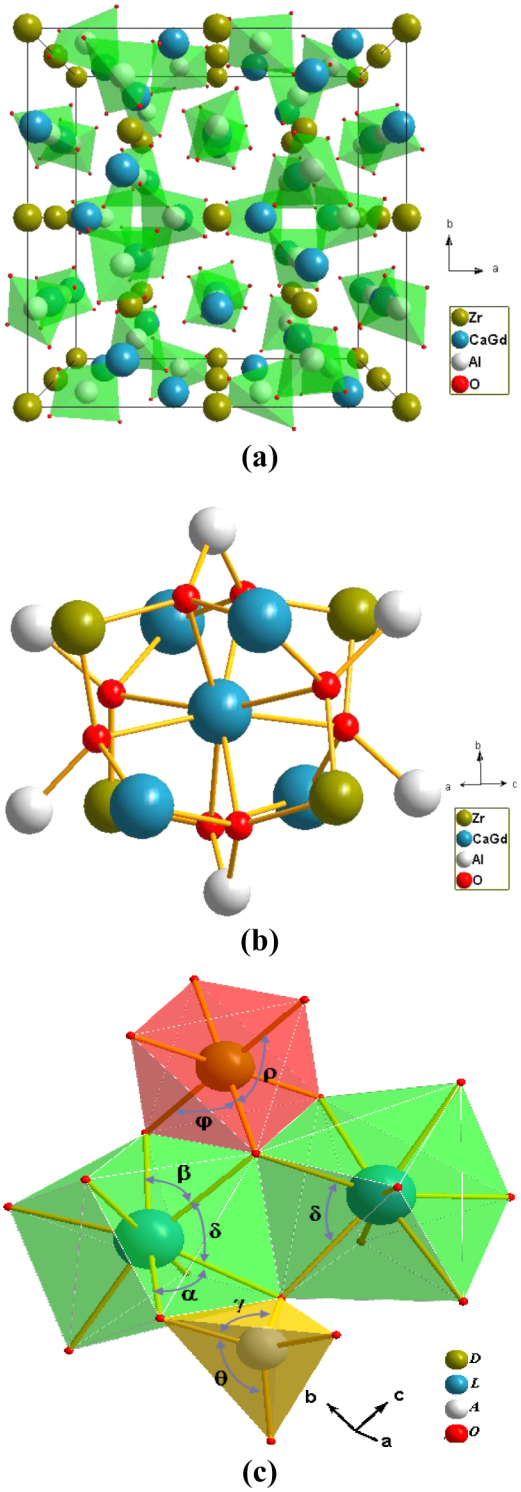

Figure 2. (a) Unit-cell representation of $Ca_2GdZr_2(AlO_4)_3$; (b) coordination geometry of Ca/Gd in $Ca_2GdZr_2(AlO_4)_3$; and (c) LO_8 dodecahedron, AO_4 tetrahedron, and DO_6 octahedron, and the selected bond angles in $Ca_2GdZr_2(AlO_4)_3$.

(^{2}D) can be distinguished from the PLE spectrum of the CGZA:0.02Ce^{3+}. The splitting of the ^2E_g can be estimated as 5345 cm^{-1}, and the barycenter of ^2E_g is determined as 26 650 cm^{-1}. Furthermore, the position of $^2A_{1g}$ can be determined as 23 980 cm^{-1}, and thus the spectroscopic red-shift $D(A)$[27] relative to the centroid position 51 230 cm^{-1} of 5d (^{2}D) state of Ce^{3+} as a free ion is about 25 360 cm^{-1}. Comparing the

Table 4. Selected Bond Lengths (Å) and Bond Valence Sums (BVS) for CGZA[a]

L-Dodecahedron	
Gd/Ca−O#5	2.403(2)
Gd/Ca−O#10	2.403(2)
Gd/Ca−O	2.403(2)
Gd/Ca−O#11	2.403(2)
Gd/Ca−O#12	2.535(2)
Gd/Ca−O#13	2.535(2)
Gd/Ca−O#1	2.535(2)
Gd/Ca−O#14	2.535(2)
BVS of L(Ca^{2+}/Gd^{3+})	Ca = 2.017, Gd = 2.642
D-Octahedron	
Zr−O#1	2.085(2)
Zr−O#2	2.085(2)
Zr−O#3	2.085(2)
Zr−O#4	2.085(2)
Zr−O#5	2.085(2)
Zr−O#6	2.085(2)
BVS of D(Zr^{4+})	4.015
A-Tetrahedron	
Al−O#16	1.777(2)
Al−O	1.777(2)
Al−O#10	1.777(2)
Al−O#17	1.777(2)
BVS of A(Al^{3+})	2.819

[a]Symmetry transformations used to generate equivalent atoms: (#1) $y - 1/4, x + 1/4, -z + 1/4$, (#2) $x - 1/4, z + 3/4, y - 1/4$, (#3) $-x + 3/4, -z + 3/4, -y + 3/4$, (#4) $-z + 1/4, y + 1/4, -x + 3/4$, (#5) $z + 1/4, -y + 5/4, x - 1/4$, (#6) $-y + 3/4, -x + 5/4, z + 1/4$, (#7) $-x + 1/2, -y + 3/2, -z + 1/2$, (#8) $z + 1/2, x + 1/2, y - 1/2$, (#9) $-y + 1, z + 1/2, -x + 1/2$, (#10) $-x + 1/2, y + 0, -z + 0$, (#11) $-z + 1/4, -y + 5/4, -x + 1/4$, (#12) $-y + 3/4, x + 1/4, z - 1/4$, (#13) $-z + 1/2, -x + 1, y - 1/2$, (#14) $z + 0, -x + 1, -y + 1/2$, (#15) $x, y + 1/2, -z$, (#16) $z + 1/4, -y + 3/4, -x + 1/4$, (#17) $-z + 1/4, -y + 3/4, x - 1/4$, (#18) $x, y - 1/2, -z$.

Table 5. Selected Angles (deg) of CGZA, YAG, and GdAG Crystals

polyhedron	angle	YAG[5]	GdAG[5]	CGZA
dodecahedron	α (O−L−O)	71.833	71.850	68.889
	β (O−L−O)	67.905	67.802	71.470
	δ (O−L−O)	73.575	74.066	72.251
octahedron	φ (O−D−O)	86.633	86.957	87.615
	ρ (O−A−O)	93.367	93.043	92.385
tetrahedron	γ (O−A−O)	99.981	100.599	99.825
	θ (O−D−O)	114.415	114.081	114.499

absorption and emission bands originating from the transitions between $^2F_{5/2}$ and $^2A_{1g}$, the Stokes shift E_s of $^2A_{1g}$ in CGZA:Ce^{3+} can be determined to be 3489 cm^{-1}. The 5d (^{2}D) barycenter shift ε_c of Ce^{3+} in CGZA can be estimated by the following expression:[27−30]

$$\varepsilon_c = 1.79 \times 10^{13} \sum_{i=1}^{N} \frac{\alpha_{sp}^{i}}{(R_i - 0.6\Delta R)^6} \quad (1)$$

$$\alpha_{sp} = 0.33 + \frac{4.8}{\chi_{av}^2} \quad (2)$$

dx.doi.org/10.1021/ic500153u | Inorg. Chem. 2014, 53, 6607−6614

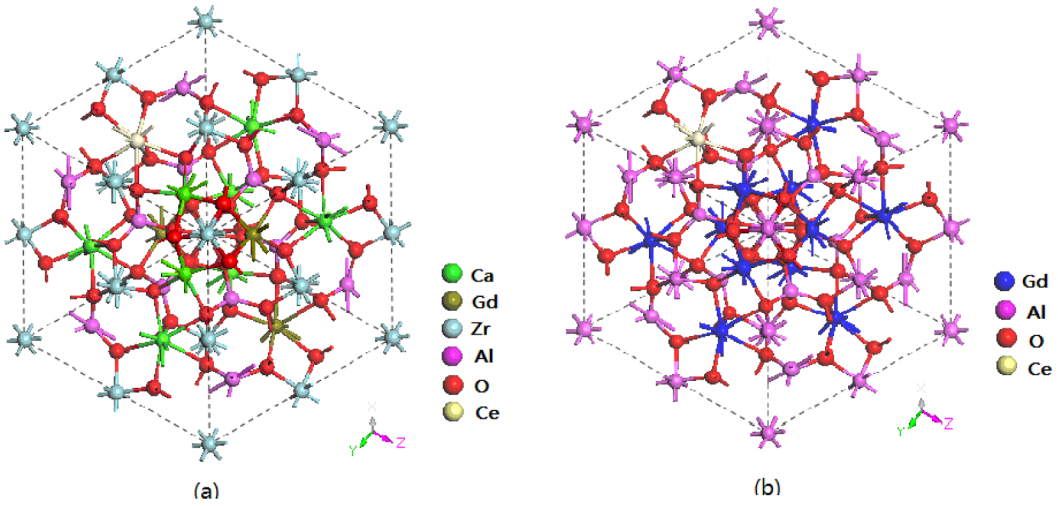

Figure 3. Supercell models for (a) $Ca_2GdZr_2(AlO_4)_3:Ce^{3+}$ and (b) $Gd_3Al_5O_{12}:Ce^{3+}$.

Table 6. Calculated Mulliken Populations and Bond Lengths of CGZA:Ce^{3+} and GdAG:Ce^{3+}

crystal	bond		population (e)	length (Å)
CGZA:Ce	L−O	Ca−O	0.03−0.11	2.3840−2.9095
		Gd−O	0.12−0.22	2.3866−2.7835
		Ce−O	0.15−0.23	2.4453−2.6830
	D−O	Zr−O	0.37−0.42	2.0954−2.1648
	A−O	Al−O	0.44−0.52	1.7744−1.8382
GdAG:Ce	L−O	Gd−O	0.13−0.25	2.3115−2.8635
		Ce−O	0.13−0.18	2.4636−2.7799
	D−O	Al−O	0.30−0.36	1.9609−2.0768
	A−O	Al−O	0.45−0.49	1.8125−1.8670

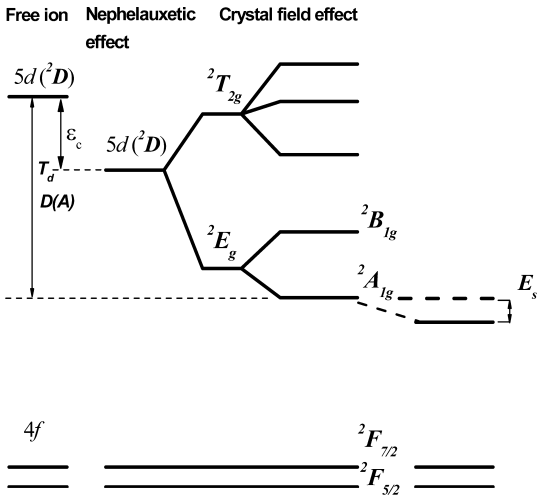

Figure 4. Energy level scheme for Ce^{3+} in garnet.

$$\chi_{av} = \frac{\sum_i n_i z_i \chi_i}{\sum_i n_i z_i} \quad (3)$$

where R_i is the Ce^{3+}−anion distance in the undistorted lattice, N represents the number of anions coordinated to Ce^{3+}, ΔR is the difference in ionic radii for the cation at L site and Ce^{3+}, χ_{av} is the weighted average of the cation electronegativity in a given oxide host lattice, n_i is the number of cations of type i with charge $+z_i$, and χ_i is Pauling type electronegativity values.[31] The 5d (^{2}D) barycenter shift ε_c of Ce^{3+} in CGZA is estimated as 17

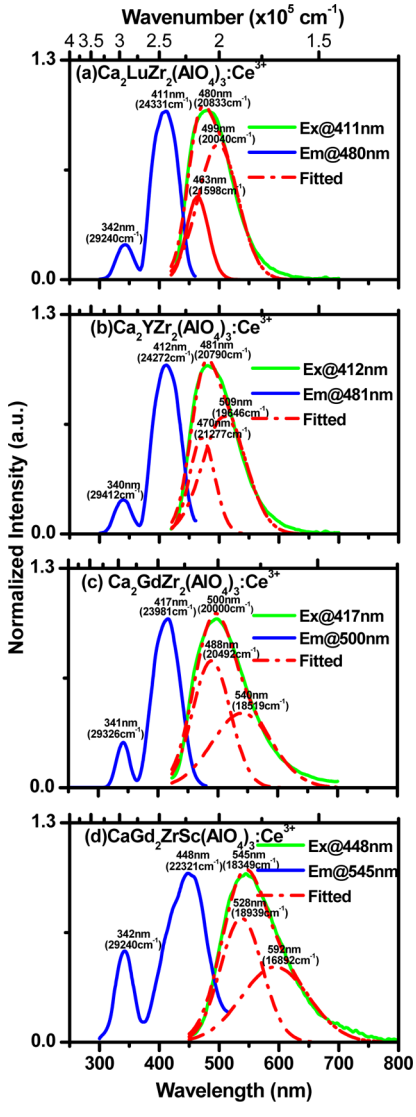

Figure 5. Normalized PL and PLE spectra of (a) $Ca_2LuZr_2(AlO_4)_3:Ce^{3+}$; (b) $Ca_2YZr(AlO_4)_3:Ce^{3+}$; (c) $Ca_2GdZr_2(AlO_4)_3:Ce^{3+}$; and (d) $CaGd_2ZrSc(AlO_4)_3:Ce^{3+}$.

dx.doi.org/10.1021/ic500153u | Inorg. Chem. 2014, 53, 6607−6614

380 cm^{-1}, which is larger than that of the typical garnets YAG:Ce^{3+} (14 250 cm^{-1}) and GdAG:Ce^{3+} (ε_c = 14 160 cm^{-1}). The T_d position thus can be estimated as 33 850 cm^{-1} relative to the centroid position 51 230 cm^{-1} of 5d (^{2}D) state of Ce^{3+} as a free ion. The energy difference between the barycenters of ^2E_g and T_d is about 1.5 times the energy difference between the barycenters of $^2T_{2g}$ and T_d in cubic coordination;[32] that is, $T_d - {}^2E_g = 1.5({}^2T_{2g} - T_d)$, and the barycenter of $^2T_{2g}$ therefore can be calculated as 38 650 cm^{-1} and thus the splitting between the $^2T_{2g}$ and ^2E_g levels represented by the phenomenological parameter $10D_q$ is determined as 12 000 cm^{-1}. The $10D_q$ of CGZA:Ce^{3+} is smaller than that of GdAG:Ce^{3+} (19 080 cm^{-1}). The larger ε_c and smaller $10D_q$ of Ce^{3+} in CGZA than those in GdAG, respectively, are related to the larger covalent character of Ce−O in CGZA as discussed in section 3.3.

Figure 6 shows the normalized PL spectra of CGZA:$x$$Ce^{3+}$ with x = 0.01−0.12 under excitation at 415 nm. The peak of PL

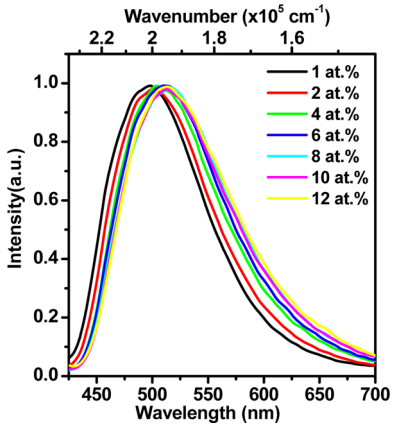

Figure 6. Normalized PL spectra for $Ca_2Gd_{(1-x)}Zr_2(AlO_4)_3$:$x$$Ce^{3+}$ (x = 0.01, 0.02, 0.04, ...0.12).

band shifts to longer wavelength from 499 nm for x = 0.01 to 514 nm for x = 0.12. The emission intensity of samples obtained by integrating the relative emission bands for CGZA:$x$$Ce^{3+}$ (x = 0.01, 0.02, 0.04, ...0.12) measured at the same condition is shown in Figure 7. It can be found that the maximum emission is at x = 0.02.

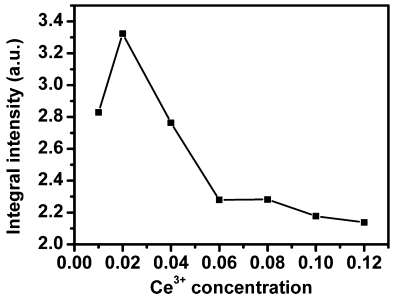

Figure 7. Relative integrated emission intensities for $Ca_2Gd_{(1-x)}Zr_2(AlO_4)_3$:$x$$Ce^{3+}$ (x = 0.01, 0.02, 0.04, ...0.12).

3.5. Tuning Spectral Properties of Ce^{3+}-Doped CGZA-Based Isostructural Phosphors. The emission color of Ce^{3+}-doped phosphors can be tuned by adjusting the composition of host or codoping the other activators.[33,34] Figure 5a, b, d shows a series of the PL and PLE spectra of CGZA-based isostructural garnet phosphors studied in this work. The emission color of these phosphors as shown in Figure 8 could be tuned from blue (peak at 480 nm with CIE chromaticity coordinate at (x = 0.16,

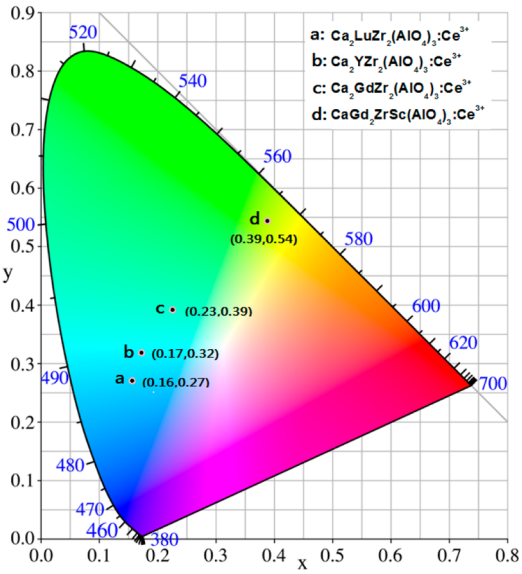

Figure 8. CIE coordinates of $Ca_2Lu_{0.98}Zr_2(AlO_4)_3$:0.02$Ce^{3+}$, $Ca_2Y_{0.98}Zr_2(AlO_4)_3$:0.02$Ce^{3+}$, $Ca_2Gd_{0.98}Zr_2(AlO_4)_3$:0.02$Ce^{3+}$, and $CaGd_{1.98}ZrSc(AlO_4)_3$:0.02Ce^{3+}.

y = 0.27)) to green-yellow (peak at 545 nm with CIE chromaticity coordinate at (x = 0.39, y = 0.54)) with the L and D sites occupied by Lu^{3+}, Y^{3+}, Gd^{3+}, and Sc^{3+}, respectively. The emission peak wavelength, 5d (^{2}D) barycenter shift ε_c, phenomenological parameter $10D_q$, splitting of ^2E_g, the barycenter of ^2E_g, spectroscopic red-shift $D(A)$, and the Stokes shift E_s of the Ce^{3+}-doped CGZA-based isostructural phosphors as well as REAG:Ce^{3+} (RE = Lu, Y, and Gd) phosphors for comparison are summarized in Table 7.

The 5d (^{2}D) barycenter shifts ε_c and phenomenological parameters $10D_q$ of Ce^{3+} in REAG:Ce^{3+} are very close, respectively, which may be due to the similar electronegativity of RE^{3+}. This result also allows one to deduce that the ε_c and $10D_q$ of Ce^{3+} in CREZA:Ce^{3+} are also similar and are about 17 400 and 12 000 cm^{-1}, respectively.

In garnet, the ^2E_g of Ce^{3+} is not degenerated in the crystal field of D_2 point symmetry, and it is not necessary to consider the typical Jahn−Teller effect, but the $E_g \times e_g$ Jahn−Teller mode as a coupling still strongly influences the splitting of ^2E_g. With larger cation occupying the L sites in the garnet, the tetragonal distortions of CeO_8 (LO_8) cube, which is related to the symmetric bending of Ce−O(L−O) bonds with the $e_g\theta$ irreducible representation, would be enhanced.[21,39−43] Therefore, the splitting of ^2E_g would be increased with the radius of L ion obviously due to the Jahn−Teller coupling effect.[39,40] As expected, the splitting of ^2E_g in CREZA:Ce^{3+} (RE = Lu, Y, and Gd) increases with the radius of RE^{3+} ion, which is similar to that in REAG:Ce^{3+} phosphors. It is also worth noting that the splittings of ^2E_g in CREZA:Ce^{3+} garnet phosphors are smaller than those in REAG:Ce^{3+} garnet phosphors, which may be mainly due to the larger covalent character of Ce−O in CREZA:Ce^{3+} and the difference in the shapes of CeO_8 (LO_8) dodecahedron in these garnets as discussed in section 3.2. Partly substituting the Zr^{4+} by Sc^{3+} at the D sites and Ca^{2+} by Gd^{3+} at the L sites to form CGZSA:Ce^{3+} phosphors seemly decreases the covalent character of the Ce^{3+} and O^{2-} ligand and

dx.doi.org/10.1021/ic500153u | Inorg. Chem. 2014, 53, 6607−6614

Table 7. Spectral Properties for the Ce^{3+}-Doped CGZA and Some Other Garnet Crystals

phosphor	peak of emission (nm)	ε_c[a] (cm^{-1})	$10D_q$ (cm^{-1})	splitting of ^2E_g (cm^{-1})	barycenter of ^2E_g (cm^{-1})	$D(A)$ (cm^{-1})	E_s (cm^{-1})	quantum yield	ref
CLuZA:Ce^{3+}	480			4909	26 790	25 010	2773	49.53%	this work
CYZA:Ce^{3+}	481			5140	26 840	25 070	2995	43.25%	this work
CGZA:Ce^{3+}	500	17 380	12 000	5345	26 650	25 360	3489	40.26%	this work
CGZSA:Ce^{3+}	545			6918	25 780	27 020	3382	13.39%	this work
LuAG:Ce^{3+}	504	14 300	18 800	6664	25 650	27 019	2201	84%	8, 30, 37, 52
YAG:Ce^{3+}	535	14 250	18 880	7600	25 650	26 650	3209	88%	8, 24, 30, 35, 36, 52
GdAG:Ce^{3+}	565	14 160	19 280	8352	25 500	28 018	3623		30, 38

[a]Calculated value based on model $\varepsilon_c = 1.79 \times 10^{13} \sum_{i=1}^{N}((\alpha_{sp}^i)/((R_i - 0.6\Delta R)^6))$ proposed by P. Dorenbos in refs 27−30.

thus increases the splitting of the ^2E_g because the distortion of CeO_8 (LO_8) polyhedrons would be decreased due to the introduction of more Gd^{3+} ions, which lead to a smaller average cation radius at L sites.

The spectroscopic red-shift $D(A)$ is determined by the splitting of the 5d (^2D) state and the barycenter shift of 5d (^2D) state as compared to free ion. Because the ε_c and $10D_q$ of Ce^{3+} in CREZA:Ce^{3+} are similar, respectively, the splitting of ^2E_g may dominate the difference of $D(A)$ in CREZA:Ce^{3+}. Therefore, the $D(A)$ in CREZA:Ce^{3+} would increases with the radius of RE^{3+} as does ^2E_g. The larger covalent character of Ce−O in CREZA:Ce^{3+} would lower the 5d (^2D) barycenter but decrease the splitting more due to the crystal field and Jahn−Teller coupling effect existing simultaneously; the spectroscopic red-shift $D(A)$ in CREZA:Ce^{3+} is therefore generally smaller than that in REAG:Ce^{3+}.

The Stokes shift E_s is caused by the lattice relaxation.[44] The E_s increases with the radius of RE^{3+} in both CREZA:Ce^{3+} and REAG:Ce^{3+} due to the increasing of distortion of CeO_8 (LO_8) polyhedrons, which leads to the stronger electron−phonon interaction.[45,46]

3.6. Thermal Quenching of Luminescence and Quantum Yields of Ce^{3+}-Doped CGZA-Based Isostructural Phosphors. Temperature dependence of relative integral emission intensities related to the transitions from the lowest-lying level $^2A_{1g}$ to the $^2F_{7/2}$ and $^2F_{5/2}$ multiplets for CREZA:Ce^{3+} and CGZSA:Ce^{3+} are shown in Figure 9. The thermal quenching properties of phosphor are related to the active energy barriers ΔE_a[47−50] for nonradiative relaxation processes. Stronger electron−phonon interaction and smaller energy difference between excited and ground state means a lower ΔE_a and a stronger nonradiative process.[47−49] For CREZA:Ce^{3+} phosphors, the luminescence temperature quenching of Ce^{3+} enhances with the radius of RE^{3+} due to the enhancement of electron−phonon interaction caused by the increasing of distortion of CeO_8 (LO_8) polyhedrons. In fact, the larger distortion of CeO_8 (LO_8) polyhedrons in CGZA-based garnet phosphors caused by introducing larger Ca^{2+} to L-sites of the garnets also leads to that the temperature quenching of Ce^{3+}-doped CGZA-based garnet phosphors is more serious than that of REAG:Ce^{3+}.[51,52] The quenching of CGZSA:Ce^{3+} is stronger than that of CGZA:Ce^{3+}, which indicated that the ΔE_a of CGZSA:Ce^{3+} decreases due to the smaller energy difference between the lowest 5d excited state and 4f ground state.

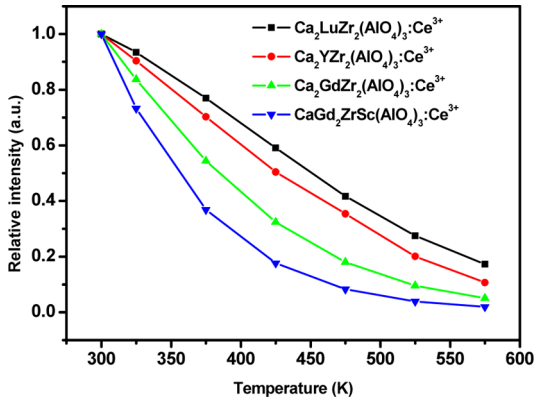

Figure 9. Temperature dependence of photoluminescence intensity on $Ca_2Lu_{0.98}Zr_2(AlO_4)_3$:$0.02Ce^{3+}$, $Ca_2Y_{0.98}Zr_2(AlO_4)_3$:$0.02Ce^{3+}$, $Ca_2Gd_{0.98}Zr_2(AlO_4)_3$:$0.02Ce^{3+}$, and $CaGd_{1.98}ZrSc(AlO_4)_3$:$0.02Ce^{3+}$ phosphors.

The quantum yields of CGZA-based phosphors measured at room temperature are given in Table 7 for comparison. The quantum yield is also related to the ΔE_a, so it would be lower in the phosphor with stronger luminescence thermal quenching.

4. CONCLUSIONS

In this work, a series of Ce^{3+}-doped aluminate phosphors containing zirconium MREZA:Ce^{3+} (M = Ca, Sr, Ba and RE = La, Gd, Y, Lu) and CGZSA:Ce^{3+} have been synthesized by the solid-state reaction method. The compounds CGZA, CLuZA, CYZA, and CGZSA crystallize in cubic system with space group $Ia\bar{3}d$, but many impurity phases exist in CSGZA, CBGZA, and CLaZA. The Mulliken bonding population analyses of the CGZA:Ce^{3+} as well as GdAG:Ce^{3+} for comparison show that the covalent character of Ce−O bonds in CGZA:Ce^{3+} is larger than that in GdAG:Ce^{3+}. The photoluminescence properties of CGZA:xCe^{3+} ($0.01 \le x \le 0.12$) were investigated, and the maximum emission occurred at $x = 0.02$. The tuning spectral properties of Ce^{3+}-doped CGZA-based isostructural phosphors by substituting the cations with Y^{3+}, Lu^{3+}, and Sc^{3+} were analyzed. The splitting of ^2E_g in CREZA:Ce^{3+} (RE = Lu, Y, and Gd) increases as the radius of RE^{3+} increasing. The ε_c and $10D_q$ of Ce^{3+} in CREZA:Ce^{3+} are similar, and are about 17 400 and 12 000 cm^{-1}, respectively. The splitting of ^2E_g may dominate the difference of $D(A)$ in CREZA:Ce^{3+}, and the $D(A)$ in CREZA:Ce^{3+} therefore increases with the radius of RE^{3+} as does ^2E_g. The splitting of the ^2E_g in $CaGd_2ZrSc(AlO_4)_3$:Ce^{3+} (CGZSA:Ce^{3+}) phosphors increases seemly due to the decreasing of the covalent character of the Ce−O. The E_s also increases with the radius of RE^{3+} in both CREZA:Ce^{3+} and REAG:Ce^{3+} due to the increasing of distortion of LO_8 polyhedrons. Thermal quenching properties of Ce^{3+}-doped CGZA-based isostructural phosphors are analyzed. For CREZA:Ce^{3+} phosphors, the increasing of the radius of RE^{3+}

dx.doi.org/10.1021/ic500153u | Inorg. Chem. 2014, 53, 6607−6614

decreases the active energy barriers for nonradiative relaxation processes and results in a enhancement of thermal quenching. The quenching of CGZSA:Ce^{3+} is stronger than that of CGZA:Ce^{3+}, which is mainly due to the smaller energy difference between the lowest 5d excited state and 4f ground state.

■ ASSOCIATED CONTENT

Ⓢ Supporting Information

CIF data. This material is available free of charge via the Internet at http://pubs.acs.org.

■ AUTHOR INFORMATION

Corresponding Author

*Tel.: +86-591-83776990. Fax: +86-591-83714946. E-mail: huyd@fjirsm.ac.cn.

Notes

The authors declare no competing financial interest.

■ ACKNOWLEDGMENTS

This work has been supported by the Science and Technology Major Project of Fujian Province (Grant no. 2011HZ0001-2).

■ REFERENCES

(1) Nakamura, S.; Mukai, T.; Senoh, M. *Appl. Phys. Lett.* **1994**, *64*, 1687−1689.
(2) Schubert, E. F.; Kim, J. K. *Science* **2005**, *308*, 1274−1278.
(3) Krupa, J. C.; Queffelec, M. *J. Alloys Compd.* **1997**, *250*, 287−292.
(4) Dorenbos, P. *J. Lumin.* **2002**, *99*, 283−299.
(5) Euler, F.; Bruce, J. A. *Acta Crystallogr.* **1965**, *19*, 971−978.
(6) Shimomura, Y.; Honma, T.; Shigeiwa, M.; Akai, T.; Okamoto, K.; Kijima, N. *J. Electrochem. Soc.* **2007**, *154*, J35−J38.
(7) Blasse, G.; Bril, A. *Philips Res. Rep.* **1967**, *22*, 481−504.
(8) Setlur, A. A.; Heward, W. J.; Gao, Y.; Srivastava, A. M.; Chandran, R. G.; Shankar, M. V. *Chem. Mater.* **2006**, *18*, 3314−3322.
(9) Sheldrick, G. M. *SHELXS-97: Program for the Solution of Crystal Structure*; University of Gottingen: Gottingen, Germany, 1997.
(10) Sheldrick, G. M. *SHELXL-97: Program for the Solution of Crystal Structure*; University of Gottingen: Gottingen, Germany, 1997.
(11) Mulliken, R. S. *J. Chem. Phys.* **1955**, *23*, 1833−1846.
(12) Segall, M.; Linda, P.; Probert, M.; Pickard, C.; Hasnip, P.; Clark, S.; Payne, M. *Materials Studio CASTEP version 2*, 2002.
(13) Segall, M.; Linda, P.; Probert, M.; Pickard, C.; Hasnip, P.; Clark, S.; Payne, M. *J. Phys.: Condens. Matter* **2002**, *14*, 2717−2744.
(14) Mizuno, M.; Yamada, T.; Noguchi, T. *J. Ceram. Soc. Jpn.* **1977**, *85*, 374−379.
(15) Mizuno, M.; Yamada, T.; Noguchi, T. *J. Ceram. Soc. Jpn.* **1978**, *86*, 360−364.
(16) Shishido, T.; Okamura, K.; Yajima, S. *J. Am. Ceram. Soc.* **1978**, *61*, 373−375.
(17) Brown, I. D. The Bond-Valence Method; An Empirical Approach to Chemical Structure and Bonding. In *Structure and Bonding in Crystals*; O'Keeffe, M., Navrotsky, A., Eds.; Academic Press Inc.: New York, 1981; Vol. *II*.
(18) Drofenik, M.; Golic, L. *Acta Crystallogr., Sect. B* **1979**, *35*, 1059−1062.
(19) Jorgensen, C. K. *Absorption Spectra and Chemical Bonding in Complexes*; Pergamon Press: Oxford, UK, 1962.
(20) Jorgensen, C. K. *Modern Aspects of Ligand Field Theory*; North-Holland Pub. Co.: Amsterdam, Netherlands, 1971.
(21) Bersuker, I. B. *The Jahn-Tellet Effect*; Cambridge University Press: Cambridge, UK, 2006.
(22) Zhao, M. G.; Xu, J. A.; Bai, G. R.; Xie, H. S. *Phys. Rev. B* **1983**, *27*, 1516−1522.
(23) Miniscalco, W. J.; Pellegrino, J. M.; Yen, W. M. *J. Appl. Phys.* **1978**, *49*, 6109−6111.
(24) Robbins, D. J. *J. Electrochem. Soc.* **1979**, *126*, 1550−1555.
(25) Randic, M. *J. Chem. Phys.* **1962**, *36*, 2094−2097.
(26) Burdett, J. K.; Hoffmann, R.; Fay, R. C. *Inorg. Chem.* **1978**, *17*, 2553−2568.
(27) Dorenbos, P. *J. Lumin.* **2000**, *91*, 155−176.
(28) Dorenbos, P. *Phys. Rev. B* **2002**, *65*, 235110-1−235110-6.
(29) Dorenbos, P. *J. Lumin.* **2003**, *105*, 117−119.
(30) Dorenbos, P. *Phys. Rev. B* **2001**, *64*, 125117-1−125117-12.
(31) Pauling, L. *The Nature of the Chemical Bond*; Cornell University Press: New York, 1960.
(32) Cotton, F. A. *Chemical Applications of Group Theory*; Wiley Interscience: New York, 1990.
(33) Geng, D. L.; Lian, H. Z.; Shang, M. M.; Zhang, Y.; Lin, J. *Inorg. Chem.* **2014**, *53*, 2230−2239.
(34) Li, G. G.; Geng, D. L.; Shang, M. M.; Peng, C.; Cheng, Z. Y.; Lin, J. *J. Mater. Chem.* **2011**, *21*, 13334−13344.
(35) Holloway, W. W., Jr.; Kestigian, M. *Phys. Lett. A* **1967**, *25*, 614−615.
(36) Ivanovskikh, K. V.; Ogieglo, J. M.; Zych, A.; Ronda, C. R.; Meijerink, A. *ECS J. Solid State Sci. Technol.* **2013**, *2*, R3148−R3152.
(37) Zhong, J. P.; Liang, H. B.; Su, Q.; Zhou, J. Y.; Wang, J. Y. *Trans. Nonferrous Met. Soc. China* **2009**, *19*, 1628−1633.
(38) Tien, T. Y.; Gibbons, E. F.; DeLosh, R. G.; Zacmanidis, P. J.; Smith, D. E.; Stadler, H. L. *J. Electrochem. Soc.* **1973**, *120*, 278−281.
(39) Seijo, L.; Barandiaran, Z. *Opt. Mater.* **2013**, *35*, 1932−1940.
(40) Wu, J. L.; Gundiah, G.; Cheetman, A. K. *Chem. Phys. Lett.* **2007**, *441*, 250−254.
(41) Grinberg, M.; Sikorska, A.; Kaczmarek, S. *J. Alloys Compd.* **2000**, *300−301*, 158−164.
(42) Burns, R. G. *Mineralogical Applications of Crystal Field Theory*, 2nd ed.; Cambridge University Press: Cambridge, UK, 1993.
(43) Henderson, B.; Imbusch, G. F. *Optical Spectroscopy of Inorganic Solids*; Clarendon Press: Oxford, UK, 1989.
(44) Huang, K.; Rays, A. *Proc. R. Soc. A* **1950**, *204*, 406−423.
(45) Clerc, F.; Battaglia, C.; Bovet, M.; Despont, L.; Monney, C.; Cercellier, H.; Garnier, M. G.; Aebi, P. *Phys. Rev. B* **2006**, *74*, 155114−1−155114−7.
(46) Espinosa, A.; Otero-Leal, M.; Rivadulla, F.; Rivas, J.; de Andres, A. *J. Lumin.* **2008**, *105*, 992−994.
(47) Born, M.; Huang, K. *Dynamical Theory of Crystal Lattices*; Oxford University Press: Oxford, UK, 1954.
(48) Huang, K. *Prog. Phys.* **1981**, *1*, 31−84 (in Chinese).
(49) Luo, Z. D.; Huang, Y. D.; Chen, X. Y. *Spectroscopy of Solid-State Laser and Luminescent Materials*; Nova Science Publishers, Inc.: New York, 2007.
(50) Chiang, C. C.; Tsai, M. S.; Hon, M. H. *J. Electrochem. Soc.* **2008**, *155*, B157−B162.
(51) Bachmann, V.; Ronda, C.; Meijerink, A. *Chem. Mater.* **2009**, *21*, 2077−2084.
(52) Birkel, A.; Denault, K. A.; George, N. C.; Doll, C. E.; Hery, B.; Mikhailovsky, A. A.; Birkel, C. S.; Hong, B. C.; Sechadri, R. *Chem. Mater.* **2012**, *24*, 1198−1204.